Food and Chemical Toxicology 161 (2022) 112819

Contents lists available at ScienceDirect

Food and Chemical Toxicology

journal homepage: www.elsevier.com/locate/foodchemtox

Beauvericin (BEA) and enniatin B (ENNB)-induced impairment of mitochondria and lysosomes - Potential sources of intracellular reactive iron triggering ferroptosis in Atlantic salmon primary hepatocytes

Sofie Søderstrøm [*], Kai K Lie [1], Anne-Katrine Lundebye, Liv Søfteland

Institute of Marine Research (IMR), Bergen, Norway

ARTICLE INFO

Handling Editor: Dr. Jose Luis Domingo

Keywords:
Beauvericin
Enniatin B
RNA sequencing Analysis
Mitochondrial impairment
Lysosomal impairment
Ferroptosis

ABSTRACT

Beauvericin (BEA) and enniatin B (ENNB) are emerging mycotoxins frequently detected in plant-based fish feed. With ionophoric properties, they have shown cytotoxic potential in mammalian models. Sensitivity in fish is still largely unknown. Primary hepatocytes isolated from Atlantic salmon (*Salmo salar*) were used as a model and exposed to BEA and ENNB (0.05–10 μM) for 48 h. Microscopy, evaluation of cell viability, total ATP, total H_2O_2, total iron content, total Gpx enzyme activity, and RNA sequencing were used to characterize the toxicodynamics of BEA and ENNB. Both mycotoxins became cytotoxic at $\geq$ 5 μM, causing condensation of the hepatocytes followed by formation of blister-like protrusions on the cell's membrane. RNA sequencing analysis at sub-cytotoxic levels indicated BEA and ENNB exposed hepatocytes to experience increased energy expenditure, elevated oxidative stress, and iron homeostasis disturbances sensitizing the hepatocytes to ferroptosis. The present study provides valuable knowledge disclosing the toxic action of these mycotoxins in Atlantic salmon primary hepatocytes.

1. Introduction

Plant-based feed ingredients are a source of novel contaminants to farmed fish. Traditional salmon feed ingredients, e.g., fishmeal and fish oil, have largely been replaced with vegetable feed ingredients making the feed more ecologically and economically sustainable (Ytrestøyl et al., 2015). Mycotoxins are secondary metabolites synthesized by crop molds, whereupon the use of mold-infested cereal grains and pulse crops for meal- and oil extraction can result in mycotoxins entering feed- and food production. Ingested mycotoxins have caused illness (mycotoxicosis) and even death in livestock and humans (Hussein and Brasel, 2001). The introduction of mycotoxins into aquafeeds from plant-based feed ingredients raises a concern regarding fish feed safety (Bernhoft et al., 2013b).

A study on mycotoxin levels in fish feeds in Kenya reported a high prevalence of several "emerging mycotoxins" (Jestoi, 2008), especially enniatin B (ENNB) but also beauvericin (BEA) (Mwihia et al., 2020). BEA and ENNs have been included in routine screening in the official annual fish feed surveillance program in Norway since 2016. Rapeseed oil has been identified as a major source of ENNB contamination in fish feed, whereas wheat- and corn gluten are sources of both BEA and ENNB (Sanden et al., 2017; Sele et al., 2018, 2019; Ørnsrud et al., 2020). ENNs and BEA have been found in the liver and fillets of commercially important fish species (e.g., sea bass (*Dicentrarchus labrax*), sea bream (*Sparus aurata*), Atlantic salmon (*Salmo salar*), and rainbow trout (*Oncorhynchus mykiss*)) (Tolosa et al., 2014, 2017). However, since existing toxicity data for BEA and ENNB are insufficient for establishing maximum contents, these mycotoxins are currently not legislatively regulated in feed or food (Lindblad et al., 2013; Bernhoft et al., 2013b; Vaclavikova et al., 2013). The occurrence of BEA and ENNB in salmon feed has highlighted the need for more knowledge regarding their potential chronic effects on fish health (Sanden et al., 2017; Sele et al., 2018, 2019; Ørnsrud et al., 2020; Bernhoft et al., 2013a). Toxicity studies on mycotoxins in fish species are limited, especially in salmonids. Atlantic salmon appear to be sensitive to dietary deoxynivalenol (DON) (Moldal et al., 2018), while Rainbow trout have been shown to be sensitive to dietary aflatoxin (Williams, 2012) and DON (Hooft et al., 2011). However, data on the dietary toxicity of BEA and ENNB in salmon and other fish are lacking. Advancing our understanding of the cellular toxicity of mycotoxins may improve the prediction of possible adverse effects in fish.

* Corresponding author.
E-mail address: sofie.soderstrom@hi.no (S. Søderstrøm).
[1] https://www.researchgate.net/profile/Kai-Lie/research.

https://doi.org/10.1016/j.fct.2022.112819
Received 5 July 2021; Received in revised form 7 January 2022; Accepted 10 January 2022
Available online 15 January 2022

Abbreviations

Enniatin B (ENNB)
Beauvericin (BEA)
Deoxynivalenol (DON)
Ochratoxin A (OTA)
Reactive oxygen species (ROS)
Ferric iron (Fe^{3+})
Ferrous iron (Fe^{2+})
Adenosine triphosphate (ATP)
3-(4,5-dimethylthiazol-2-yl)-2,5-diphenyl tetrazolium bromide (MTT)
Ribonucleic acid (RNA)
RNA integrity number (Rin)
Hydrogen Peroxide (H_2O_2)
Differentially expressed genes (DEGs)
Tricarboxylic acid cycle (TCA cycle)
Peroxisome proliferator-activated receptors (PPARs)
Polyunsaturated fatty acid (PUFA)
Glutamate cysteine ligase (Gcl)
Glutathione synthetase (Gss)
Glutathione reductase (Gsr)
Reduced glutathione (GSH)
Oxidized glutathione (GSSG)
Glutathione peroxidase (Gpx)
Glutathione peroxidase 4 (Gpx4)
Polyunsaturated fatty acid (PUFA)

Few studies have assessed the cytotoxicity of BEA or ENNB in fish. However, BEA has been shown to exhibit high cytotoxicity in cell lines derived from rainbow trout hepatoma (RTH-149) (EC_{50} = 5.96 μg/mL), desert topminnow (*Poeciliopsis lucida*) hepatocellular carcinoma (PLHC-1) (EC_{50} = 2.89 μg/mL) (García-Herranz et al., 2019), and rainbow trout gill (RTgill-W1) (EC_{50} = 3.01 μg/mL) (Bernal-Algaba et al., 2021). Furthermore, García-Herranz et al. (2019) found that fish cell lines exhibited similar sensitivity to that of a rat (*Rattus norvegicus*) cell line (H4IIE) (EC_{50} = 1.80 μg/mL). Results from a mammalian cell model (Caco-2) have shown that both mycotoxins are cytotoxic at lower micro molar concentrations (BEA IC_{50} = 12.80 μM, ENNB IC_{50} = 11.7 μM) (Prosperini et al., 2013a, 2013b). These mycotoxins have also been shown to initiate mammalian cell death in an apoptotic or necrotic manner (Prosperini et al., 2013a, 2013b; Jonsson et al., 2016).

BEA and ENNB can act as ionophores, which has been suggested to be their underlying mechanism of toxicity (Mallebrera et al., 2018; Prosperini et al., 2017). Owing to their chemical structure, BEA and ENNB are lipophilic and prone to incorporation in the lipid bilayers of cellular- and organelle membranes (Kouri et al., 2003; Kamyar et al., 2004; Tonshin et al., 2010). When incorporated, these mycotoxins can disrupt the otherwise strictly regulated transport of ions. For example, BEA and ENNB have been shown to affect the transport of several essential cations (e.g., K^+, Na^+, and Ca^{2+}) either by acting as ion carriers or as cation-selective channels (Ivanov et al., 1973; Hilgenfeld and Saenger, 1985; Kouri et al., 2003, 2005; Kamyar et al., 2004). The proposed mode of toxic action of BEA and ENNB is the disruption of ion and pH homeostasis, which in turn disturbs normal cell- and organelle function (Kamyar et al., 2004; Kouri et al., 2005; Tonshin et al., 2010; Wu et al., 2018).

A variety of sub-lethal toxic effects have been reported from studies with different mammalian cell models. For example, BEA and ENNB have been demonstrated to depolarize mitochondrial transmembrane potential and to uncouple oxidative phosphorylation in rat liver mitochondria (Tonshin et al., 2010). BEA has been shown to cause mitochondria uncoupling and to deplete ATP in myocytes from guinea pig (*Cavia porcellus*) (Kouri et al., 2005). Either one or both mycotoxins have generated oxidative stress (i.e., the formation of reactive oxygen species (ROS) and/or lipid peroxidation) in exposed mammalian cell lines (Prosperini et al., 2013a, 2013b; Ivanova et al., 2012; Mallebrera et al., 2015; Klarić et al., 2007; Ferrer et al., 2009). Furthermore, BEA has been shown to inhibit the acyl-CoA cholesterol acyltransferase enzyme (ACAT) (Tomoda et al., 1992), and to affect the antioxidant system by decreasing glutathione levels in porcine-, rodent-, and human cell lines (Klarić et al., 2007; Mallebrera et al., 2014; Prosperini et al., 2013a). ABC transporter proteins such as ABCB1 and ABCG2 have, however, exhibited the ability to diminish the cytotoxic effects of BEA and ENNs in human cells (Dornetshuber et al., 2009).

Since Atlantic salmon is an important farmed fish species in Norway, the aim of this study was to generate salmon-specific toxicity data of these emerging mycotoxins. In compliance with the 3R principles (replace, reduce, refine), primary hepatocyte cells isolated from Atlantic salmon were used to assess the cytotoxicity of BEA and ENNB. With non-targeted transcriptomics, the aim was to discover the mycotoxins' mode of action by identifying affected pathways. The results of this study will be valuable for improving our understanding of how BEA and ENNB affect fish health and feed safety.

2. Materials and methods

2.1. Mycotoxins

The mycotoxins, beauvericin (BEA, cas 26048-05-5) and enniatin B (ENNB, cas 917-13-5) used in the exposure experiments were purchased from AdipoGen® (AdipoGen® Life Sciences, Nordic BioSite, Oslo, Norway). BEA and ENNB were dissolved individually in dimethyl sulfoxide (DMSO) (Sigma-Aldrich, Oslo, Norway) to constitute a 15 mM stock solution from which dilutions were made. In an initial experiment, the mycotoxins were exposed as single compounds at concentrations of 0.05, 0.5, 1.5, 2.5, and 5 μM, and in a follow-up experiment at 0.05, 2.5, and 5 μM. In both experiments, 0.1% DMSO was used as a control. In the cell viability assays (xCELLigence, MTT, Neutral red) exposure to 10 μM was also included. The mycotoxin stock solutions, as well as the control, were diluted in Leibovitz L-15 medium w/o phenol red (ThermoFisher, Oslo, Norway) supplemented with 9% FBS (Sigma-Aldrich, Oslo, Norway), 1% salmonid serum (#N82800F, Meridian Life Science, Inc. Memphis, USA), 1% Antibiotic Antimycotic Solution (10000 units penicillin, 10000 μg streptomycin, and 25 μg amphotericin per mL) (Sigma-Aldrich, Oslo, Norway), and from here on denoted as suppl. L-15.

2.2. Ethical statement

In these experiments, for the first time, a clonal all-male Atlantic salmon line was used that has been developed at the Institute of Marine Research (IMR), Bergen, Norway (Fjelldal et al., 2020). Using all-male salmon reduced the use of fish to a minimum (no females had to be discarded) thus favoring the 3R principles. All work was carried out in agreement with the current national *animal welfare act - the regulation on animal experimentation* approved by the Norwegian Animal Research Authority and overseen by the Norwegian Food Safety Authority (FOTS ID, 19351).

2.3. Isolation and exposure of primary cultures of Atlantic salmon hepatocytes

Atlantic salmon hepatocytes were isolated using the two-step liver

perfusion method described by Søfteland et al. (2009) under semi-sterile (hepatocyte cell isolation) and sterile (cell work) conditions. Prior to the start of the experiments, the fish were maintained in a fish-holding facility at IMR. Six juvenile fish weighing between 216 and 326 g were used in the initial experiment (analyses: xCELLigence, MTT, ATP, H_2O_2, and RNA sequencing), and four juveniles weighing between 136 and 193 g were used in the follow-up experiment (analyses: MTT, Neutral red, Iron, and Gpx). In brief, during the first step the liver was perfused through the hepatic vein with a perfusion buffer containing 17 mM EDTA (Sigma-Aldrich, Oslo, Norway) to clear the liver of blood, followed by the second perfusion step where the liver was digested by the addition of collagenase VIII (0.1 mg/mL) (Sigma-Aldrich, Oslo, Norway) to the perfusion buffer. The digested liver was transferred to a Petri dish with ice cold 1X PBS and gently pulled apart using tweezers, followed by pipetting the tissue suspension up and down using a 5-mL syringe. The homogenate was filtered through a 100 μm nylon mesh. The isolated hepatocytes were washed thrice with cold 1X PBS through centrifugation at 50 G for 5 min, and finally resuspended in suppl. L-15. Before seeding the hepatocytes, viability was confirmed to be $\geq$ 80% with trypan blue staining (BioRad) using a Bürker counting chamber (Tiefe 0.100 mm, 0.0025 mm^2) under a microscope (Axiovert 40 CFL, Carl Zeiss, Jena, Germany). Hepatocytes harvested from each of the biological replicate salmon (initial: n = 6, follow-up: n = 4) were seeded in precoated (2 $\mu g/cm^2$ laminin, Sigma-Aldrich, Oslo, Norway) well culture plates. Hepatocytes were incubated at 10 °C, without any additional O_2 or CO_2 throughout the duration of the experiments (MIR-554-PE Cooled Incubator, PHCbi, Etten-Leur, The Netherlands).

According to the methodology-optimization done by Søfteland et al. (2009), the hepatocytes were acclimatized for 48 h prior to exposure (given fresh suppl. L-15 after 24 h). On the third day, the hepatocytes were exposed to the mycotoxins for the following 48 h (given fresh exposure solution on the fourth day) (for exposure regimes see *2.1 Mycotoxins*). On the fifth and final day of the experiments, the predetermined endpoints were measured (initial: xCELLigence, MTT, ATP levels, H_2O_2 levels/follow-up: MTT, Neutral red, Iron levels, Gpx enzyme activity). All spectrophotometric measurements were done using a VICTOR X5 plate reader (PerkinElmer, Waltham, Massachusetts, USA). The hepatocytes from the initial experiment intended for RNA sequencing were immediately lysed in RLT Plus buffer (Qiagen, Crawley, UK) and stored at −80 °C until further processing for RNA extraction and purification.

2.4. Real-time viability assessment – xCELLigence

Real-Time Cell Analysis (RTCA) was carried out using the xCELLigence system (ACEA Biosciences, San Diego, CA, USA) according to manufactures' instructions to quantify biological factors, such as changes in cell morphology and the strength of the cells-substrate adhesion to the surface throughout the entire exposure duration (48 h). Primary hepatocytes (n = 6 per experimental condition) were seeded with a density of 2×10^5 cells per well in a 96-well electronic microtiter plate (E-plate) (ACEA Biosciences, San Diego, CA, USA), and cultured in 0.2 mL suppl. L-15. The hepatocytes were left to settle for 30 min before starting to monitor the response. As the cells adhere to the bottom of the E-plate with electrodes integrated into the bottom, the cell-electrode impedance was measured via the xCELLigence RTCA single plate (SP) station kept inside the incubator. After exposing the hepatocytes to BEA and ENNB, measurements were taken every 2 min during the first 12 h, then every 15 min of the remaining exposure time). Cell index (CI) values were then derived from the recorded cell-electrode impedance data, giving quantitative information about the cells' biological status and viability. The CI was normalized against the last point before starting the mycotoxin exposure (i.e., CI at a given time/CI at reference point (put to 1) using the RTCA Software v1.2.1.

2.5. Viability assessment - mitochondrial metabolic activity and lysosomal function

An MTT and a Neutral red-based *In Vitro* Toxicology assay kit (Sigma-Aldrich, St Louis, Missouri, USA) were used to assess the hepatocytes' mitochondrial metabolic activity and lysosomal function, respectively. Primary hepatocytes (initial experiment n = 6 and follow-up experiment n = 4 per experimental condition) were seeded with a density of 2×10^5 cells per well in a 96-well cell-culture plate (Nunc™, Roskilde, Denmark) and cultured in 0.2 mL suppl. L-15. The BEA and ENNB exposure solutions were removed after 48 h, and the cells were added either MTT (5 mg/mL) or solution neutral red (0.33%) (20 μL of MTT or neutral red solution was added to 200 μL fresh suppl. L-15) and placed back into the incubator for 4 h. Thereafter, the dye solutions were replaced with an assay solubilizing solution and stored at 4 °C in an airtight bag over the weekend. Spectrophotometric measurement of MTT was done at absorbance (abs) 570 nm, and neutral red at abs 540 nm (both corrected against background at 690 nm). The mycotoxins were regarded as cytotoxic when their concentration elicited a reduction in hepatocyte viability exceeding 30% relative to the control (ISO, 2009).

2.6. RNA extraction and sequencing

Hepatocytes for RNA sequencing were seeded with a density of 72×10^5 cells per well in 6-well cell-culture treated plates (Corning® Costar®, Sigma-Aldrich, Oslo, Norway) and cultured in 3 mL suppl. L-15. After 48 h exposure to BEA or ENNB, the cells were immediately lysed in RLT Plus buffer (Qiagen, Crawley, UK), flash frozen and stored at −80 °C. A RNeasy Plus Mini Kit (Qiagen, Crawley, UK) was used according to supplier's protocol to extract and purify total RNA from the cell lysate. Purified RNA was diluted in 30 μL RNase-free MilliQ H_2O and stored at −80 °C until further analysis. RNA quantity and purity was measured using NanoDrop™ (One Microvolume UV–Vis Spectrophotometer, Thermo Fisher Scientific™, Waltham, MA, USA). The 260/280 and 260/230 nm ratios were 2.07 ± 0.03 and 2.38 ± 0.04, respectively, indicating pure samples of satisfactory quality (n = 6 per experimental condition, mean ± STD). RNA integrity was evaluated on an RNA 6000 Nano LabChips with an Agilent 2100 Bioanalyzer (Agilent Technologies, Palo Alto, CA, USA) according to manufacturer's protocol. The RNA integrity numbers (Rin) were 10.0 ± 0.0 (indicating non-degraded RNA) for all samples intended for RNA sequencing. RNA samples (2 μg) were sent to the Norwegian Sequencing Centre (NSC) (www.sequencing.uio.no) in Oslo, Norway, where the sequencing and library preparation were performed. DNA libraries were prepared using 90 ng total RNA input to the TruSeq Stranded mRNA Library Prep Kit (Illumina, San Diego, California, USA) per manufacturer's protocol. For multiplexing, standard Illumina adaptors were used. The libraries were sequenced using the NextSeq Illumina platform (Illumina, San Diego, California, USA) according to the manufacturer's instructions, generating single end 75 bp read libraries with an average library size of 10 ± 2 million reads. A total of 48 libraries were generated, 24 for BEA and 24 for ENNB, where (based on cell viability results) three experimental conditions below cytotoxic levels (0.05, 0.5, 2.5 μM) plus control (0.1% DMSO) were selected for RNA sequence analysis, n = 6 per experimental condition. Raw reads were submitted to the gene expression omnibus https://www.ncbi. nlm.nih.gov/geo/(GEO accession: GSE193374).

2.7. RNA sequencing read mapping and differential gene expression

TrimGalore 0.4.2 wrapper tool (https://github.com/FelixKrueger/TrimGalore) was used for removing adaptors and quality trimming, applying the default parameters. Library quality was investigated using fastQC included in the TrimGalore wrapper.

Individual libraries were mapped to the Atlantic salmon genome (RefSeq Assembly ICSASG_v2) using the Hisat2 short read aligner

version 2.0.4 (Kim et al., 2015) and the Atlantic salmon NCBI gene annotation file (Salmon_salar, January 24, 2017 GCA_000233375.4_ICSASG_v2_genomic.gff), with a mapping efficiency rate of 87 ± 9%. Transcript levels for the individual libraries were estimated using FeatureCounts (Liao et al., 2014) of the Subread package (http://subread.sourceforge.net/). Read counts were normalized using Bioconductor R package (version 3.4.4) DESeq2 (version 1.18.1) (Love et al., 2014). Genes of which fewer than five samples had gene counts below or equal to 10 reads were excluded from further analysis prior to normalization. Differential gene expression was analyzed using Qlucore Omics Explorer 3.5 (Qlucore AB, Lund, Sweden). Prior to statistical analysis, pre-processed RNA sequencing data were log2 transformed.

2.8. Determination of cellular levels of ATP and H_2O_2

A Luminescent ATP Detection Assay Kit (ab113849, Abcam, Cambridge, UK), and a ROS-Glo™ H_2O_2 Assay (Promega, Madison, Wisconsin, USA) were used to measure total levels of ATP and hydrogen peroxide (H_2O_2), respectively. Hepatocytes (n = 6 per experimental condition) were seeded with a density of 2×10^5 cells per well in a 96-well cell-culture plate (Nunc™, Roskilde, Denmark) and cultured in 0.2 mL suppl. L-15. After 48 h exposure to BEA or ENNB, the hepatocytes were assayed according to supplier procedures (the non-lytic protocol for H_2O_2). ATP and H_2O_2 levels were measured through luminescence spectrophotometry in black opaque 96F-well OptiPlates (PerkinElmer, Waltham, Massachusetts, USA).

2.9. Determination of cellular iron and Gpx activity

An iron assay kit (ab83366) and a Glutathione peroxidase (Gpx) assay kit (ab102530) (Abcam, Cambridge, MA, USA) were used to assess the cellular ferric (Fe^{3+}) and ferrous (Fe^{2+}) iron levels and total Gpx activity, respectively. Hepatocytes (n = 4 per experimental condition) were seeded with a density of 26×10^5 cells per well in 12-well cell-culture plates (Corning® Costar®, Sigma-Aldrich, Oslo, Norway) and cultured in 2 mL suppl. L-15. After 48 h exposure to BEA or ENNB, the hepatocytes were washed with cold 1X PBS and harvested in either iron assay buffer, or cold Gpx assay buffer. The cells were then homogenized by pipetting (for the iron assay, cells were sonicated 3–4 short pulses at 30% amplitude, 0.5 cycle), and centrifuged at 13.000 G for 5 min at 4 °C. The supernatants were collected and assayed according to supplier procedures, using 100 μL-undiluted samples in the iron assay and 50 μL-undiluted samples in the Gpx assay. Spectrophotometric measurement of Fe^{3+} and Fe^{2+} was done at abs 570 nm, and Gpx activity at abs 340 nm after 5 min incubation at room temperature.

2.10. Statistics - transcriptomics and IC_{50}

Qlucore Omics Explorer 3.5 "eliminated factor" option was used to control for confounding factors in the transcriptomic analysis related to the isolation of primary hepatocytes (i.e., time of day, the person doing the isolation, differences in the basal level of transcription) prior to statistical analysis. The Two Group Comparison embedded in the Qlucore Omics Explorer 3.5 was used for significance analysis in the pairwise comparison of each contrast (Ctrl vs BEA 0.05, Ctrl vs BEA 0.5, Ctrl vs BEA 2.5 μM, Ctrl vs ENNB 0.05, Ctrl vs ENNB 0.5, Ctrl vs ENNB 2.5 μM) ($q < 0.1$, fold change >1) and to generate scatter plots of specific DEGs. NCBI gene ID's of differentially expressed genes (DEGs) combined with fold change was used for KEGG pathway analysis, and in addition KEGG module enrichment (enrichMKEGG) analysis returning the enriched module categories (functional units, e.g., pathway modules and structural complexes) of the gene set. Significantly enriched pathways and modules were investigated using ClusterProfiler v3.12.0 and differentially expressed genes of each contrast (p.adjust <0.1). PCA plots Qlucore Omics Explorer 3.5, and The Multi Group Comparison embedded in the Qlucore Omics Explorer 3.5 was used for generating principal component analysis (PCA) plots showing the different exposure groups of each mycotoxin relative control ($q < 0.1$). Venn diagrams were created with Venny 2.1.0 (Oliveros, 2007), and GraphPad Prism v.9 (GraphPad Software Inc., Palo Alto, CA, USA) was used to display dose-response relationships in the mycotoxin-exposed primary hepatocytes measured with the different assays. Results are showed as mean ± SD (n = 6 per experimental condition, initial: xCELLigence, MTT, ATP, H_2O_2, and RNA sequencing) (n = 4 per experimental condition, follow-up: MTT, Neutral red, Iron, and Gpx). A one-way ANOVA followed by Dunnet's post hoc test ($p < 0.05$) was used to calculate significant changes in the response relative to the control.

3. Results

3.1. Viability of salmon primary hepatocytes after BEA and ENNB exposure

In the initial experiment, both BEA and ENNB produced a bell-shaped dose-response according to the xCELLigence electric cell-substrate impedance assessment (associated to cellular changes e.g., cell adhesion, surface adhesion, cell migration, morphology) (Fig. 1, A). The dose-response curve of ENNB (IC_{50} = 3.23 μM) appeared to peak at lower concentrations compared to BEA (IC_{50} = 5.05 μM) (Fig. 1, A). The impedance was reduced by 29% and 34% at 10 μM of BEA and ENNB, respectively (Fig. 1, A), and 5 μM ENNB resulted in a 26% reduction of impedance (Fig. 1, A). Results obtained with the MTT-based cell viability assay (mitochondrial metabolic activity) also indicated effects at 5 and 10 μM of ENNB (IC_{50} = 4.20 μM) as a reduction of metabolic activity in the cells by 50% and 75%, respectively (Fig. 1, B). BEA (IC_{50} = 4.97 μM) decreased the cells metabolic activity by 50% at 10 μM (Fig. 1, B). In a follow-up experiment, using a new batch of fish and exposure solutions, the neutral red-based cell viability assay indicated that both mycotoxins impair lysosomal function at 2.5, 5, and 10 μM, BEA (IC_{50} = 2.58) causing a reduction by 20, 55, and 53%, and ENNB (IC_{50} = 11.14) by 11, 25, and 49%, respectively (Fig. 1, C). The MTT assay indicated that BEA (IC_{50} = 2.57) exerted cytotoxicity at 2.5, 5, and 10 μM causing a reduction of metabolic activity by 25, 65, and 57%, respectively, and ENNB (IC_{50} = 5.66 μM) at 5 and 10 μM caused a reduction of 27 and 60%, respectively (Fig. 1, D). Due to the high cytotoxicity at 10 μM of both BEA and ENNB, this concentration was excluded from any further testing. Since the degree of cytotoxicity at 5 μM started to become questionable, this concentration was excluded from RNA sequencing analysis. However, 5 μM was retained as the highest exposure concentration for dose-response purposes in the functional analyses (i.e., ATP, H_2O_2, Iron, and Gpx).

3.2. Morphological effects of BEA and ENNB in the salmon primary hepatocytes

In the initial experiment, visual examination of hepatocytes exposed to 5 μM ENNB showed changed morphology compared to the control cells (Fig. 2, A). The cells had contracted and exhibited a different growth pattern (though still attached to the culture plate) (Fig. 2, A). Some of the hepatocytes exposed to 5 μM ENNB also appeared to have protruding blister-like features on the cell membrane. Exposure to 5 μM BEA in the initial experiment did not cause any obvious visual changes to the cell's morphology (Fig. 2, A). When assessing the RNA integrity with Bioanalyzer to ensure good RNA quality of samples for RNA sequencing, the integrity of the RNA in cells exposed to 5 μM BEA showed no signs of degradation, all samples had an RNA integrity number (Rin) = 10 (Fig. 2, A, below cell picture). Cells exposed to 5 μM ENNB also exhibited high Rin number (Rin ≥9.5) (Fig. 2, A, below cell picture). However, collectively the results from xCELLigence, MTT, and visual examination of morphology indicated that ENNB (and to some degree also BEA) was cytotoxic to the hepatocytes at the relatively low micromolar concentration of 5 μM. In the follow-up experiment, the

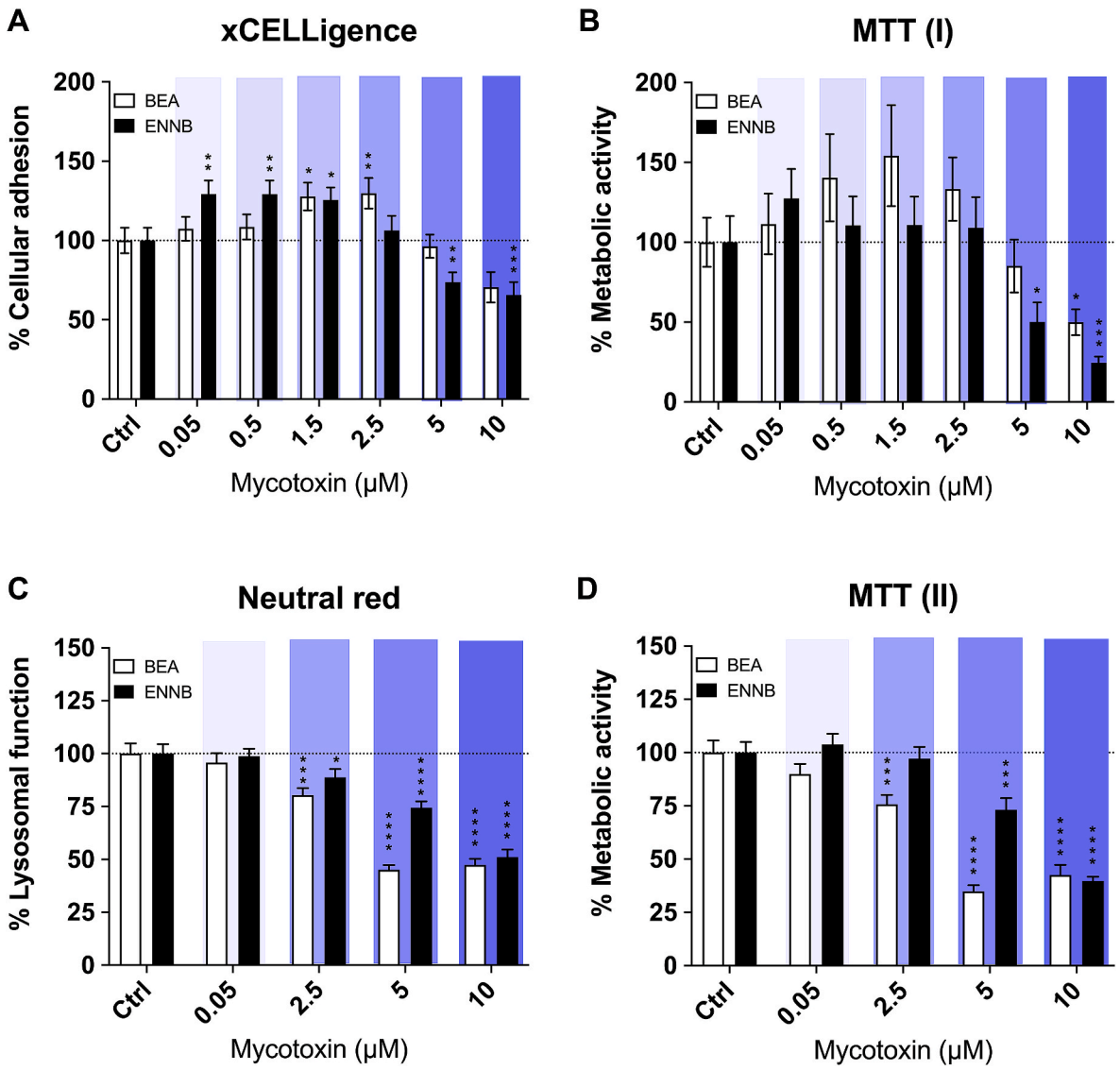

Fig. 1. Viability of primary hepatocytes exposed to BEA and ENNB. (A) xCELLigence, data shown as % cellular adhesion based on normalized cell index relative control. (B, D) MTT assay (I and II), data shown as % mitochondrial metabolic activity based on corrected abs (abs 570–690 nm) relative to control. (C) Neutral red assay, data shown as % lysosomal function based on corrected abs (abs 540–690 nm) relative to control. (A, B) n = 6. (C, D) n = 4 analyzed in duplicate. *p < 0.05, **p < 0.01, ***p < 0.001, ****p < 0.0001. (For interpretation of the references to color in this figure legend, the reader is referred to the Web version of this article.)

hepatocytes exposed to 5 μM of both BEA and ENNB exhibited obvious signs of morphological changes i.e., cell contraction and protrusion development (Fig. 2, B). The hepatocytes, which had been exposed to 2.5 μM of BEA and ENNB also exhibited altered morphology (though less obvious than in cells exposed to 5 μM), and these changes were more pronounced for BEA than ENNB (Fig. 2, B). The differences between the initial and follow-up experiment were reflected in both morphological changes and MTT results in exposed cells (Fig. 1, B). Thus, morphological changes became evident when the exposure concentration exceeded the IC_{50} established in the MTT assays. In some cases, concentrations approaching IC_{50} also produced an intermediate change in the cells.

3.3. Differential gene expression and affected pathways following BEA and ENNB exposure

RNA sequencing technology revealed differentially expressed genes (DEGs) in Atlantic salmon hepatocytes exposed to 0.05, 0.5, and 2.5 μM of BEA and ENNB. The general trend was that the number of unique DEGs increased with increasing exposure concentration of both BEA and ENNB (Fig. 3A and B). Compared to the control, BEA 0.05 μM resulted in zero DEGs, BEA 0.5 μM in 293 DEGs (53% up-, and 47% down-regulated), and BEA 2.5 μM in 364 DEGs (49% up, 51% down) (Fig. 3, A, C). Whereas ENNB 0.05 μM resulted in 48 DEGs (46% up, 54% down), ENNB 0.5 μM in 245 DEGs (56% up, 44% down), and ENNB 2.5 μM in 2614 DEGs (63% up, 37% down) (Fig. 3B–D). Thus, in the initial experiment ENNB 2.5 μM appeared to have the greatest effect on gene transcription in the exposed Atlantic salmon primary hepatocytes also resulting in a larger proportion of up-regulated DEG than down-regulated. The PCA analysis showed the relationship between the different exposures concentration of BEA and ENNB to be best explained by principal component 1 (PC1), PC1 = 50% and PC1 = 55%, respectively (Fig. 3E–F).

To elucidate how the DEGs translate into functional cellular responses, a KEGG pathway enrichment analysis was run to identify enriched metabolic- and signaling pathways. No significantly enriched pathways were observed following 0.05 μM of BEA and ENNB exposure. The enrichment analysis indicated that 0.5 μM BEA enriched the ribosome pathway (sasa03010) (Fig. 4, A), causing down-regulation of all associated DEGs (Fig. 4, B). At 2.5 μM, BEA enriched 6 pathways (Fig. 4, A). The most significantly enriched pathway following 2.5 μM BEA

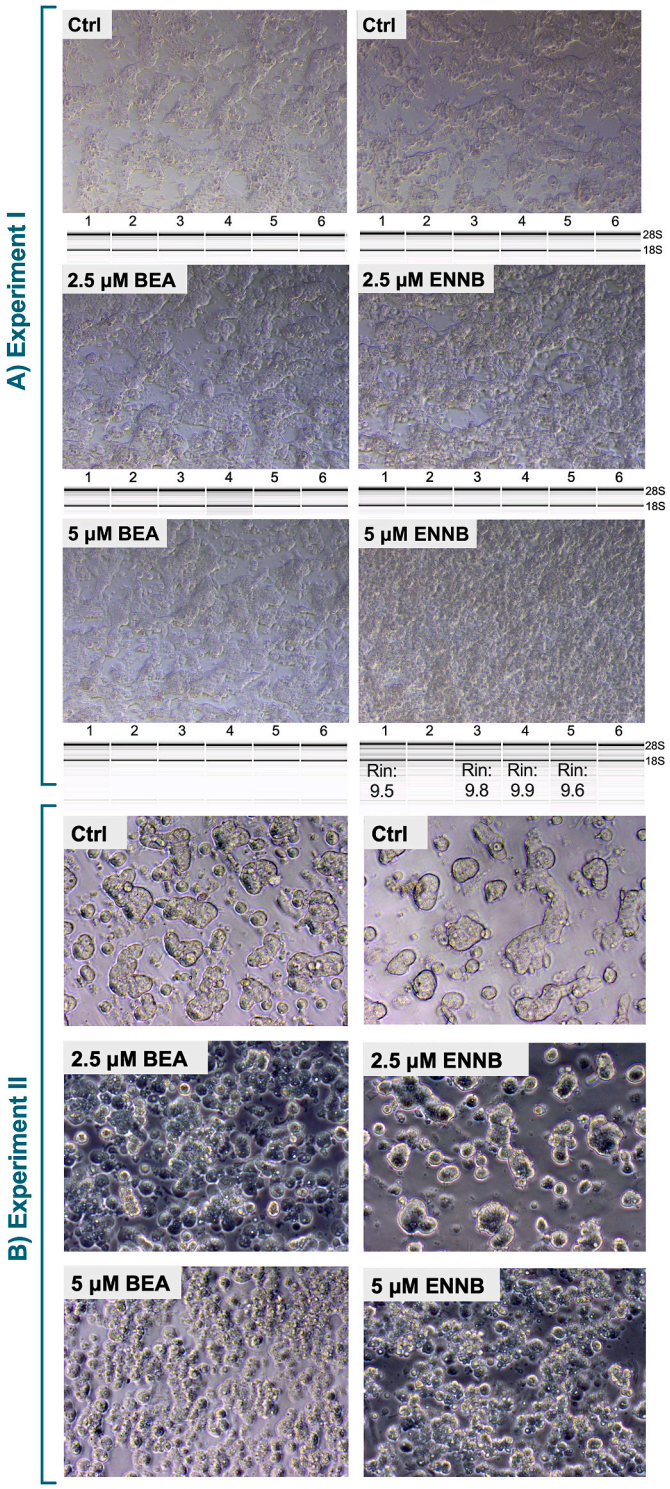

Fig. 2. Cell morphology. Primary hepatocytes imaged by light microscopy showing (A) control cells (Ctrl), and cells exposed to 2.5 and 5 µM of either BEA or ENNB (mag. 20x). RNA integrity in all 6 biological replicates is shown below cell pictures depicting 18 S and 28 S ribosomal subunit bands, RNA integrity number (Rin) = 10 if not otherwise indicated. (B) Control cells (Ctrl), and cells exposed to 2.5 and 5 µM of either BEA or ENNB (mag. 40x).

exposure was glutathione metabolism (sasa00480) (Fig. 4, A), and the transcript levels of the associated DEGs appeared to overall increase (Fig. 4, B). The number of increased and decreased DEGs attributed to ferroptosis (sasa04216) was the same, while the DEGs in the remaining pathways appeared to mainly decrease (Fig. 4, B). The top represented DEGs within glutathione metabolism with the highest increase in transcripts levels were the genes encoding glutamate cysteine ligase (Gcl) (gene: *gcl)*, and glutathione reductase (Gsr) (gene: *gsr*) (Fig. 4C and D). The DEG encoding glucose-6-phosphate1-dehydrogenase (*g6pd*) was up-regulated in the pentose phosphate pathway, while the gene encoding heme-oxygenase (*hmox*) was represented in the ferroptosis pathway (Fig. 4E and F) (for details on individual DEGs, see Supplemental Information BEA-Pathways).

Enrichment analysis of 0.5 µM ENNB indicated enhanced glycerolipid metabolism (sasa00561; Fig. 5, A), where the number of increased and decreased DEGs were equal (Fig. 5, B). At 2.5 µM, ENNB enriched 26 pathways (Fig. 5, A). The most significantly enriched pathway by 2.5 µM ENNB was the ribosome pathway (sasa03010), while the second most significant pathway was oxidative phosphorylation (sasa00190) (Fig. 5, A) (Supplemental Information Fig. S1.). All pathways affected by 2.5 µM ENNB appeared to primarily be up-regulated, with increased transcript levels of most DEGs (Fig. 5, B). The top represented DEGs within glycolysis/gluconeogenesis were the genes encoding phosphoenolpyruvate carboxykinase (Pepck) (gene: *pepck*) and glucose-6-phosphatase (G6Pase) (gene: *g6pase*) (Fig. 5C and D). The DEG encoding nuclear receptor coactivator 4 (*ncoa4*) was represented in the ferroptosis pathway (Fig. 5, E) (for details on individual DEGs, see Supplemental Information ENNB-Pathways). Affected pathways common to both mycotoxins were biosynthesis of cofactors (sasa01240), PPAR signaling pathway (sasa03320), ferroptosis (sasa04216), and pentose phosphate pathway (sasa00030) (Fig. 4, A, C). Of note, both BEA and ENNB enriched the ferroptosis pathway (sasa04216), i.e., cell death by iron-dependent lipid peroxidation (Fig. 4, A, C) and was the only enrich pathway related to regulated cell death. A detailed explanation of ferroptosis and how BEA and ENNB affected individual genes encoding key regulating proteins and rate limiting steps can be found in supplementary data (Supplemental Information Fig. S2. 1., S.2.2.).

In-depth analysis of functional units using enrichMKEGG indicated ENNB at 2.5 µM up-regulated three functional units related to central carbohydrate metabolism, four units related to ATP synthesis (representing complex III, IV, V), and one unit related to methane metabolism (Fig. 6).

3.4. Impact of BEA and ENNB on total ATP, total H_2O_2, cellular iron levels, and Gpx activity

In the initial experiment, energy production in the Atlantic salmon primary hepatocytes was assessed after exposure to BEA and ENNB by measuring the total levels of cellular ATP, as other studies have reported effects on OXPHOS. No significant changes in ATP levels were detected at concentrations lower than 2.5 µM (apart from a weak trend of a bell-shaped response), though a decline exceeding 80% was observed at 5 µM for both BEA and ENNB (Fig. 7, A). The ability of BEA and ENNB to induce the generation of reactive oxygen species was assessed by measuring H_2O_2 content in exposed cells. No significant changes in H_2O_2 levels were detected at concentrations lower than 2.5 µM (apart from a weak dose-dependent reduction, and a weak increase in 2.5 µM ENNB), while a significant reduction (≥70%) was observed for both BEA and ENNB at 5 µM (Fig. 7, B). These results showed that 5 µM BEA and ENNB drastically reduced both the levels of ATP and H_2O_2 in exposed Atlantic salmon hepatocytes.

The RNA sequencing analysis done in the initial experiment indicated that BEA affected glutathione metabolism, ENNB affected amino acid syntheses of glutathione precursors (i.e., Glycine and Cysteine), and both mycotoxins enriched the ferroptosis pathway (iron-dependent regulated cell death) (Fig. A, C). Therefore, a follow-up experiment was carried out to further evaluate whether BEA and ENNB affected cellular iron levels as well as Gpx activity, since Gpx4 is important for the defense against ferroptosis. The iron assay, where both Fe^{2+} and Fe^{3+} are measured and together they constitute the total cellular iron content, showed BEA at 5 µM significantly increased the levels of Fe^{3+} and hence

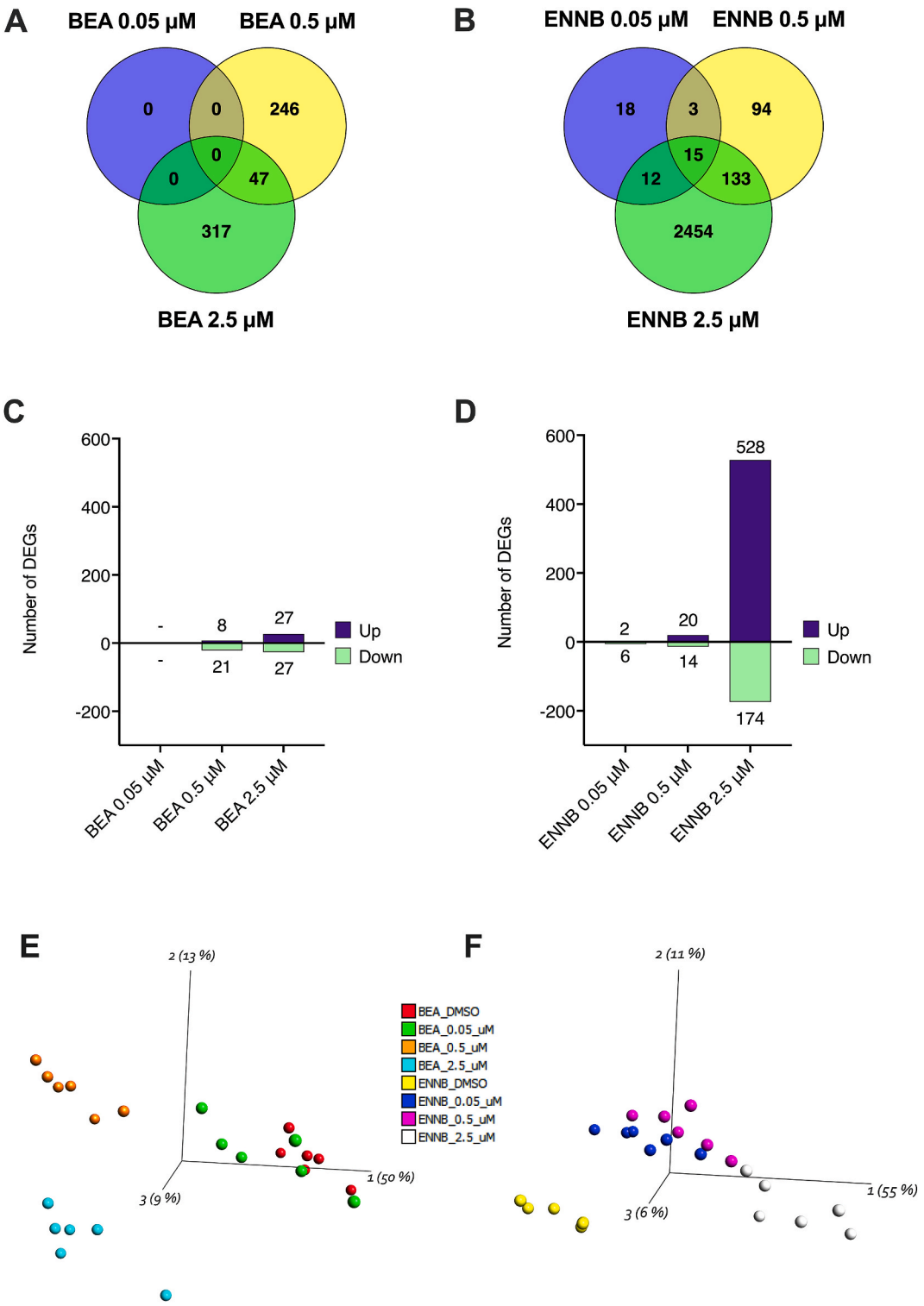

Fig. 3. Differentially expressed genes (DEGs). (A, B) Venn diagrams, (C, D) bar plots of the DEGs up- (purple) or down- (green) regulated, (E, F) PCA plots (legend indicating toxin and concentration) of exposure to three different concentrations of BEA and ENNB in relation to controls ($q < 0.1$, fold change >1.0). (For interpretation of the references to color in this figure legend, the reader is referred to the Web version of this article.)

also the total level of iron in the cells (Fig. 7. C). The Gpx activity assay showed that all three concentrations of BEA (5, 2.5 and 0.05 µM), as well as 5 and 2.5 µM of ENNB significantly increased the activity of Gpx (Fig. 7. D).

4. Discussion

The prevalence of BEA and ENNB has increased in fish feed (Ytrestøyl et al., 2015), although the sensitivity of salmon to these emerging mycotoxins remains unknown. The toxicity exerted by BEA and ENNB in the present study was in general agreement with cytotoxic effects described in other studies, such as impairing lysosomal function and

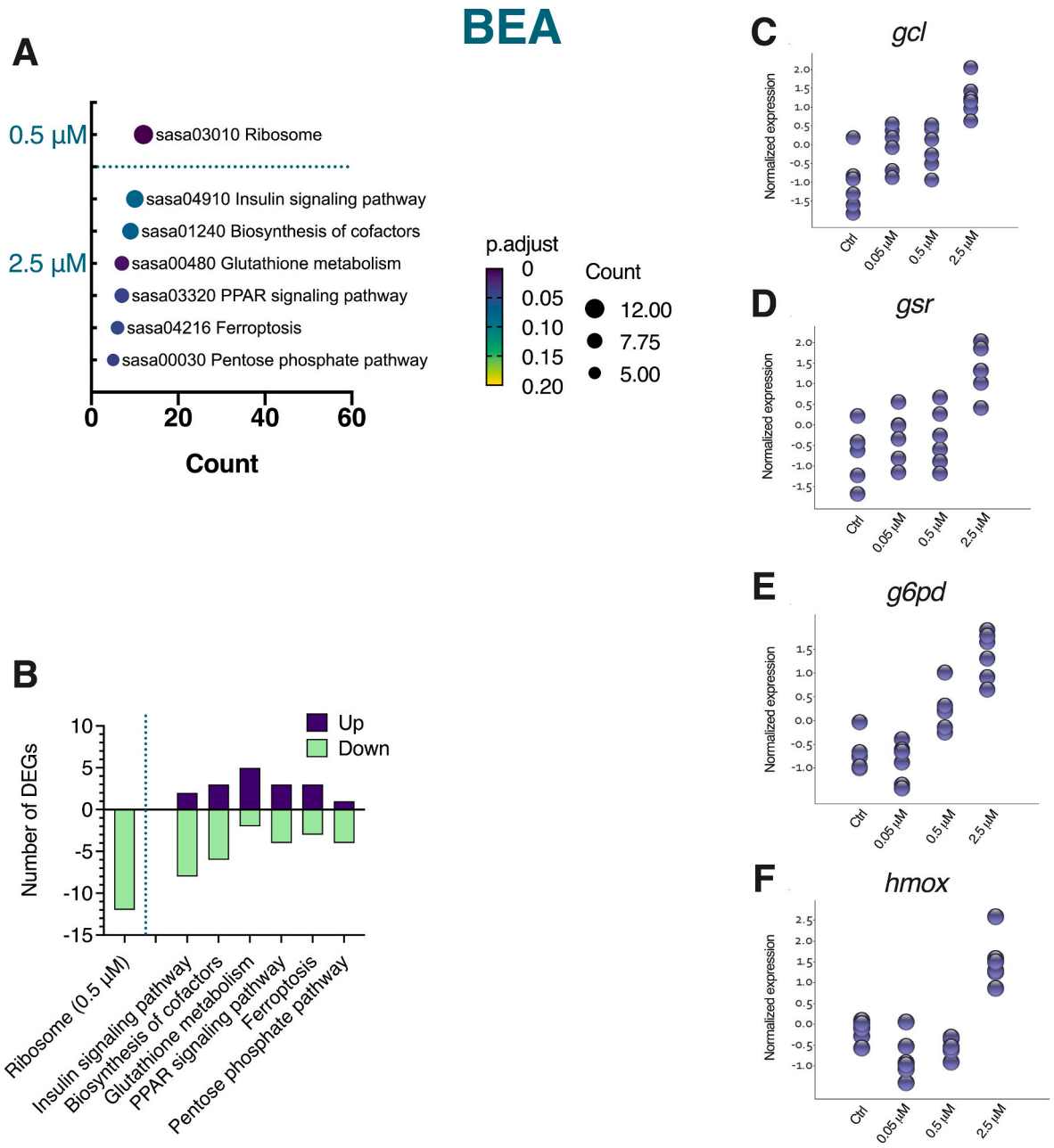

Fig. 4. KEGG pathway enrichment analysis of differentially expressed gene (DEG) counts. Enriched pathways in Atlantic salmon primary hepatocytes exposed to (A) 0.5 and 2.5 µM of BEA. X-axis and bubble size depict the count of attributed DEGs in each enriched pathway. Y-axis shows each enriched pathway where the fill colors from yellow to purple denotes the adjusted p-value (significant <0.1), the closer to purple the higher the significance. (B) Bar plot of the number of DEGs up- (purple) or down- (green) regulated, q < 0.1, fold change >1.0. (C-F) Scatter plots showing normalized expression of specific genes at the different exposure concentration including control. (For interpretation of the references to color in this figure legend, the reader is referred to the Web version of this article.)

mitochondrial metabolic activity. RNA sequencing analysis at sub-cytotoxic levels further indicated BEA and ENNB-exposed salmon hepatocytes to experience an increased energy expenditure, oxidative stress, and disturbed iron homeostasis that sensitized the hepatocytes to ferroptotic cell death.

4.1. Cytotoxicity and morphology of salmon primary hepatocytes

The cell viability assessments (xCelligence, MTT and Neutral red) indicated that both mycotoxins were highly cytotoxic to the hepatocytes already at low µM concentration. In the initial experiment of the present study, ENNB exhibited higher cytotoxicity than BEA both in terms of effects on morphology and adhesion of the cells, as well as mitochondrial metabolic activity and impaired lysosomal function. However, in the follow-up experiment, BEA appeared more cytotoxic than ENNB. Thus, the dose-responses were fish and/or exposure batch-dependent although still within a narrow µM-range. We found that BEA affected both mitochondria and lysosomes to a similar degree, while ENNB had a greater impact on mitochondrial metabolic activity than lysosomal function. Similarly, Bernal-Algaba et al. (2021), found BEA to be more cytotoxic than ENNB when evaluating lysosomal function (Neutral red), mitochondrial metabolic activity (AlamarBlue) and plasma membrane integrity (CFDA-AM) in exposed rainbow trout gill cells (RTgill-W1). In contrast to the present study, they found lysosomal function to be more affected. Whereas García-Herranz et al. (2019) reported that BEA exerted higher toxicity to mitochondrial metabolic

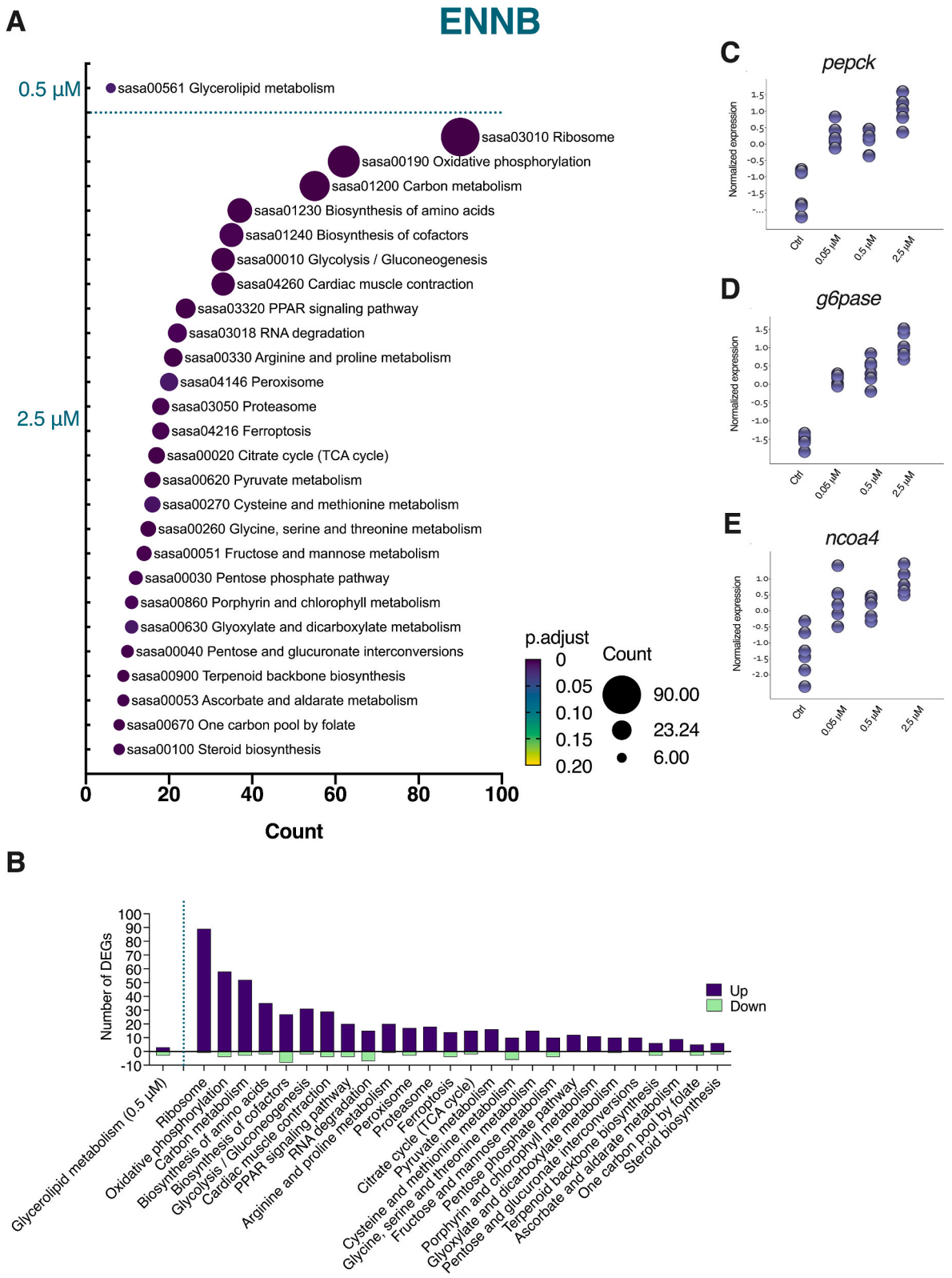

Fig. 5. KEGG pathway enrichment analysis of differentially expressed gene (DEG) counts. Enriched pathways in Atlantic salmon primary hepatocytes exposed to (A) 0.5 and 2.5 µM of ENNB. X-axis and bubble size depict the count of attributed DEGs in each enriched pathway. Y-axis shows each enriched pathway where the fill colors from yellow to purple denotes the adjusted p-value (significant <0.1), the closer to purple the higher the significance. (B) Bar plot of the number of DEGs up- (purple) or down- (green) regulated, q < 0.1, fold change >1. (C-F) Scatter plots showing normalized expression of specific genes at the different exposure concentration including control. (For interpretation of the references to color in this figure legend, the reader is referred to the Web version of this article.)

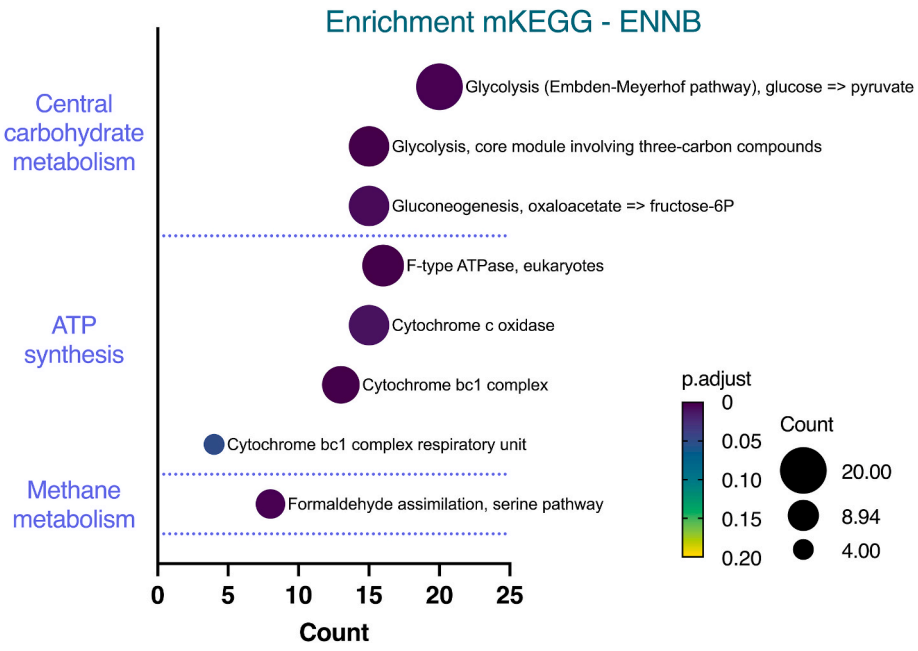

Fig. 6. EnrichMKEGG functional unit enrichment analysis of differentially expressed genes (DEGs) by 2.5 μM of ENNB. X-axis and bubble size depict the count of attributed DEGs in each functional unit. Y-axis shows significantly enriched functional (p-adjust < 0.1) units and the fill colors from yellow to purple denote statistical significance. (For interpretation of the references to color in this figure legend, the reader is referred to the Web version of this article.)

activity than to lysosomal function, or plasma membrane integrity in the rainbow trout cell line RTH-149. In line with the present study which showed BEA and ENNB to be cytotoxic at low μM concentrations to the salmon hepatocytes, both García-Herranz et al. (2019) and Bernal-Algaba et al. (2021) reported high cytotoxicity of BEA (and ENNB) especially compared to the more well-studied mycotoxins ochratoxin A (OTA) and DON. This may be of potential concern since neither BEA nor ENNB are currently legislatively regulated in feed or food (Bernhoft et al., 2013b).

4.2. *Increased energy expenditure with enhanced compensatory metabolic activity*

RNA sequencing analysis showed that ENNB produced a more pronounced dose-response than BEA, both in terms of the numbers of unique DEGs and enriched pathways. Pathway enrichment analysis at the two lowest concentrations of BEA and ENNB sequenced (0.05 and 0.5 μM) gave few or no enriched pathways, whereas 2.5 μM of the mycotoxins enriched several pathways related to energy expenditure and homeostasis in the exposed hepatocytes. At 2.5 μM, ENNB significantly up-regulated genes related to the oxidative phosphorylation pathway. The electron transport chain drives oxidative phosphorylation of ADP to ATP during mitochondrial respiration (Stockwell et al., 2020), whereas the enrichMKEGG analysis especially emphasized ENNB's effect on complex II, IV, and V of the electron transport chain. Previous mammalian *in vitro* studies have also shown BEA and ENNB to cause transcriptional changes in genes related to oxidative phosphorylation (Jonsson et al., 2016; Alonso-Garrido et al., 2018; Escrivá et al., 2018). In contrast to the ENNB-induced up-regulation of oxidative phosphorylation in the present study, the previously mentioned studies indicated primarily down-regulation of genes related to the oxidative phosphorylation pathway. Further, ENNB appeared to cause a shift in the hepatocytes' metabolic state into glucose anabolism, consuming ATP at an increased rate. The measured cellular ATP levels indicated that the hepatocytes were able to sustain increased energy expenditure at sub-cytotoxic concentrations of the mycotoxins. However, 5 μM of both BEA and ENNB caused a sharp decline in cellular ATP levels, which coincided with reduced cell viability. BEA and ENNB's ionophoric properties could potentially cause a disruption of the ion homeostasis, affecting the rate of mitochondrial respiration (i.e., ATP production) (Hajnóczky et al., 1995), or cause a depolarization of the mitochondrial membrane potential (i.e., halting ATP production) (Tonshin et al., 2010).

The glycolysis/gluconeogenesis pathway was enriched by ENNB, although gluconeogenesis seemed to be favored since the genes encoding the two rate-limiting gluconeogenic enzymes, phosphoenolpyruvate carboxykinase (Pepck) and glucose-6-phosphatase (G6Pase) (Klover and Mooney, 2004), were among the top up-regulated DEGs. This was further supported by the enrichMKEGG analysis of functional units enriched by the DEGs, which also indicated gluconeogenesis to be represented as one out of three functional units. In addition, several of the observed enriched metabolic pathways (i.e., pyruvate metabolism, TCA cycle, carbon metabolism, amino acid metabolism, PPAR signaling pathway, fructose and mannose metabolism) were implied to be up-stream events supplying precursors to gluconeogenesis (Rowsell et al., 1973; Sun et al., 2019; Klover and Mooney, 2004; Chinetti et al., 2000; Hannou et al., 2018). The production of such glucogenic precursors is ATP-dependent (Melkonian et al., 2021). In contrast to ENNB, BEA had limited effect on gluconeogenesis apart from one down-regulated DEG (fructose 1,6-bisphosphate) at 2.5 μM. Increased energy expenditure is often observed as an adaptive stress response (Manoli et al., 2007). For example, rats orally exposed to ochratoxin (OTA) exhibited disturbed energy metabolism at a transcriptional level in the liver (Qi et al., 2014).

4.3. *Oxidative stress in exposed salmon primary hepatocytes*

While oxidative phosphorylation is the main process providing the cells with ATP, it is also a significant intracellular source of reactive oxygen species (Brown et al., 2010). The transcriptional up-regulation of oxidative phosphorylation by ENNB in the present study may indicate an increased generation of reactive oxygen species. H_2O_2 levels in the hepatocytes were measured since this reactive oxygen species has the longest half-life and thus best chance of detecting (Zhao et al., 2018). However, neither BEA nor ENNB caused any significant changes in H_2O_2 levels at sub-cytotoxic levels. Only a drastic decrease in H_2O_2 was

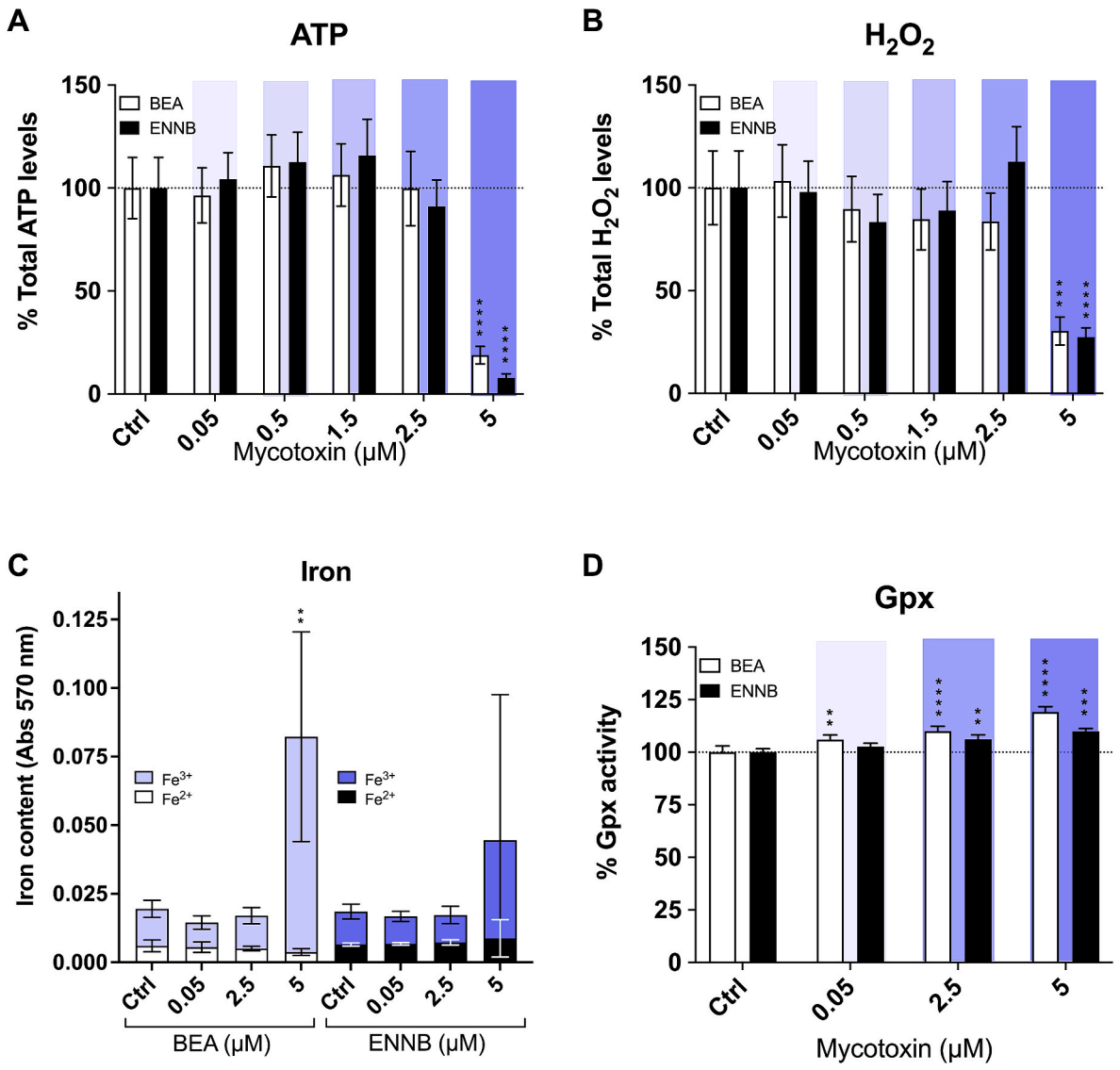

Fig. 7. Total levels of ATP, H_2O_2, Iron, and Gpx enzyme activity in salmon primary hepatocytes exposed to BEA and ENNB. (A) ATP assay, data shown as % total ATP levels based on average relative luminescence units (RLU) relative to control. (B) H_2O_2 assay, data shown as % total H_2O_2 levels based on average RLU relative to control. (C) Iron assay, data shown as cellular levels of ferrous (Fe^{2+}), and ferric (Fe^{3+}), stacked showing total iron content based on average corrected abs 570 relative to control. (D) Gpx assay, data shown as % Gpx enzyme activity based on average abs 340 nm after 5 min relative to control. (A, B) n = 6. (C, D) n = 4. **p < 0.01, ***p < 0.001, ****p < 0.0001.

observed at cytotoxic levels of both mycotoxins, which is probably correlated to the observed decline in ATP levels, and reduced cell viability at cytotoxic levels.

Inferred from the pathway enrichment analysis, BEA enriched both glutathione metabolism and biosynthesis of cofactors at sub-cytotoxic levels, where the top DEGs encoded glutathione reductase (Gsr), glutamate cysteine ligase (Gcl), and s-adenosylmethionine synthase isoform type-2 (Metk2; a synthase that activate a precursor needed to synthesize glutathione) (Lieber, 2002). Circulation of oxidized glutathione (GSSG) and reduced glutathione (GSH) through Gsr-activity, sustains the need for GSH, serving as a reducing agent for glutathione peroxidase (Gpx) during reactive oxygen species-scavenging (Lushchak, 2012; Das and Roychoudhury, 2014). Glutathione is synthesized from the precursor's cysteine, glutamate, and glycine, which are condensed into glutathione through a two-step reaction, where the first step is carried out by Gcl (Wu et al., 2004). The enrichment of peroxisomes, cysteine-, glycine-, and glyoxylate metabolism pathways by ENNB were likely up-stream events that supplied precursors needed for glutathione biosynthesis, as well as precursors for gluconeogenesis (Wu et al., 2004; Salido et al., 2012). The enrichment of the pentose phosphate pathway by both BEA and ENNB may also be related to the function of the antioxidant defense, as one of the primary products of the pentose phosphate pathway is nicotinamide adenine dinucleotide phosphate (NADPH), which is important for H_2O_2 savaging as NADPH gives reducing power to glutathione reductase (Gsr) (Chandel, 2021). The transcription of the rate-limiting enzyme, glucose-6-phosphate 1-dehydrogenase (G6pd), which directs glucose breakdown through the pentose phosphate pathway (Stanton, 2012; Tang, 2019), was up-regulated by BEA. Despite the ROS assay being unable to detect any significant increase in H_2O_2, the inferred elevation of the hepatocytes' redox state from the pathway enrichment analysis was supported by the dose-dependent increase in Gpx enzyme activity following BEA and ENNB exposure. BEA (0.1–5 μM) has previously been shown to significantly increase the Gpx activity in CHO-K1 cells (Mallebrera et al., 2014). An increased reactive oxygen species generation can distress cells and thereby trigger the onset of regulated cell death (Dixon and Stockwell, 2014).

4.4. Mitochondrial and lysosomal dysfunction – sensitizing the hepatocytes to ferroptosis?

Previous studies have described that BEA and ENNB induce apoptotic (Prosperini et al., 2013b) or necrotic cell death (Jonsson et al., 2016). Ivanova et al. (2012) on the other hand, reported that ENNB induced a cell death pathway in Caco-2 cells that did not exhibit any typical characteristics of classical apoptosis (PI/Hoechst assay) or necrosis (LDH assay). In the present study, hepatocytes exposed to cytotoxic levels of ENNB and BEA started to contract, exhibited a different growth pattern, and developed protruding blister-like features on the cell membrane consistent with the early onset of cell death. Xie et al. (2016) categorized typical morphological features of cell death into 1) necrosis - plasma membrane rupture; 2) apoptosis - rounded-up cell morphology with blebbing on plasma membrane; 3) ferroptosis - rounded-up cell morphology with intact plasma membrane free from "apoptotic" blebbing. Later studies on ferroptosis have described plasma membranes exhibiting "blisters", "ballooning" formations, or protrusions due to membrane integrity loss (Magtanong et al., 2019; Dodson et al., 2019, Van der meeren et al., 2020). These recent observations of ferroptosis are in line with the phenotype exhibited by the salmon hepatocytes exposed to cytotoxic levels of BEA and ENNB in the present study. In addition, the pathway enrichment analysis indicated that ENNB affected lipid membranes. ENNB enriched glycerophospholipid metabolism, and up-regulated the gene for the lipoprotein lipase (top DEG), which breaks down lipoproteins (e.g., triglycerides and cholesterol) into free fatty acids (Leaver et al., 2008), in the hepatocytes exposed to 0.5 μM. While at 2.5 μM, ENNB enriched terpenoid backbone synthesis producing terpenes, and steroid biosynthesis producing cholesterol via lysosomal acid lipase enzyme activity (top DEG). Both terpenes and cholesterol can be incorporated into phospholipid membranes to regulate their fluidity (Mendanha and Alonso, 2015; Nicholson et al., 2013).

The enrichment of genes related to the ferroptosis pathway in hepatocytes exposed to 2.5 μM BEA and ENNB added further support to this mode of cell death. Ferroptosis is described as an iron-dependent cell death pathway causing toxic levels of lipid peroxidation in PUFA-rich phospholipid membranes, which will propagate if not repaired by the GSH/Gpx antioxidant defense system (Dixon et al., 2012; Xie et al., 2016). Both mycotoxins affected transcript levels of key enzymes responsible for sensitizing cells to ferroptosis, such as enzymes important for polyunsaturated fatty acid phospholipid synthesis (e.g., *acsl4 and sat1*) (Yuan et al., 2016; Ou et al., 2016), and iron metabolism (e.g., *transferrin, steap3, dmt1, hmox, vdac2/3, ferritin, ncoa4*) (Paul et al., 2017; Zhang et al., 2012; Andrews, 1999; Choi and Alam, 1996; Colombini, 2004; Hou et al., 2016) (For a more detailed explanation of the ferroptosis pathway see Supplemental Information). Free Fe^{2+} is toxic and can react with H_2O_2 and, through a Fenton-like reaction, generate highly reactive hydroxyl radicals prone to cause peroxidation of PUFA-rich lipid membranes, while the iron is oxidized to Fe^{3+} (Dixon and Stockwell, 2014; Jiang et al., 2021). In the present study, cytotoxic levels of BEA caused a significant increase in Fe^{3+} in the hepatocytes, thus indicating that a Fenton reaction had occurred. Lipid membranes which have suffered peroxidation form hydrophilic pores, can further impair the barrier function of membranes (Ju et al., 2021), potentially escalating the event. Ferritin is an iron chaperone protein which prevents Fe^{2+} from reacting with hydroxyl free radicals (Paul et al., 2017), and ferritin transcription was increased by ENNB. Interestingly, ENNB also increased the transcription of the nuclear receptor coactivator 4 (*ncoa4*), which implied that iron was released from ferritin in the exposed hepatocytes. Overexpression of Ncoa4 has been shown to mediate ferritin-degradation, releasing unstable iron in fibroblasts and cancer cells which triggered the initiation of ferroptosis (Hou et al., 2016). Research suggests that stress-induced release of intracellular iron (to toxic levels) may occur from compromised iron-storing units such as lysosomes or mitochondrion (Terman and Kurz, 2013; Muñoz et al., 2016; Mena et al., 2015), and ferritin (Biasiotto et al., 2016). Thus, a plausible explanation is that the stress induced by BEA and ENNB caused an increased release of intracellular iron by damaging the lysosomes, the iron-storing ferritin, and mitochondria in the hepatocytes. Effects on lysosomes were supported by the results from the Neutral red assay showing that both mycotoxins significantly decreased lysosome function in a dose-dependent manner. Similarly, Ivanova et al. (2012) reported the loss of lysosomal integrity in ENNB-exposed Caco-2 cells. Almeida et al. (2006) demonstrated that isolated mitochondria were extremely sensitive to iron-induced lipid peroxidation, which caused permeabilization of their membranes. The observed reduction of the mitochondrial metabolic activity by both mycotoxins in the present study implied that mitochondrial iron homeostasis and retention might have been impaired. The presented data indicated that the salmon primary hepatocytes were becoming ferroptotic rather than apoptotic or necrotic. The mycotoxin aflatoxin B1 was recently shown to affect ferroptosis signaling in chicks (Zhao et al., 2021), and the mycotoxin DON caused iron imbalance in IPEC-1 cells (Lin et al., 2021). To our knowledge, this is the first time that BEA and ENNB have been associated with disruption of cellular iron homeostasis.

In this study we used the transcriptomic data for pathways enrichment analyses as a hypothesis-generating tool, to identify affected metabolic pathways that could explain the mechanisms of BEA and ENNB causing cellular responses and toxicity in the exposed hepatocytes. Since a cell's biological function is controlled through a dynamic (spatio-temporal) and complex network of signaling within and between pathways through crosstalk and feedback loops (Kholodenko, 2006), a small change in gene transcription could be important for the downstream effects (Zhan et al., 2017). With a good sample size (i.e., $n = 6$ per experimental condition) we did not wish to set a fold change cutoff criterion, at risk of losing valid data thereby failing to signify important pathways that contribute to producing the response (Zhan et al., 2017). As presented, the transcriptomics indicated that e.g., both the iron metabolism and the redox state of the exposed hepatocytes were significantly altered. Although statistical significance is not necessarily equivalent to biological relevance (Zhan et al., 2017), the independent follow-up experiment analyzing Gpx activity, lysosomal function, and cellular iron content in exposed primary hepatocytes, further corroborated our RNA-Seq generated hypothesis from the initial experiment. Whether the observed effects are secondary to the predicted primary mechanism of action of BEA and ENNB requires further studies to clarify. The level of toxicity exhibited by the exposed primary Atlantic salmon hepatocytes justifies a call for more *in vitro* and *in vivo* toxicity data in farmed Atlantic salmon to further elucidate the toxic mode of action of these prevalent mycotoxins.

5. Conclusion

Both BEA and ENNB were highly cytotoxic to Atlantic salmon primary hepatocytes, and impaired endpoints such as mitochondrial metabolic activity and lysosomal function in a dose-dependent manner. Cytotoxic levels of BEA and ENNB also caused shrinkage of the hepatocytes and the formation of protruding blister-like features on their cell membranes, consistent with the onset of cell death. At a transcriptional level, BEA and ENNB appeared to increase the hepatocytes' energy expenditure causing them to shift their metabolic state into an anabolic ATP-consuming state, and to trigger a general adaptive stress response in the hepatocytes by eliciting an increased redox balance to cope with the inflicted stress. This was supported by a dose-dependent increase in the GSH-dependent Gpx enzyme activity following exposure to both BEA and ENNB. Further, both BEA and ENNB enriched the ferroptosis pathway and measurement of intracellular iron, implying initiation of cell death through iron-dependent lipid peroxidation.

CRediT authorship contribution statement

Sofie Søderstrøm: Conceptualization, Methodology, Validation, Formal analysis, Investigation, Resources, Writing – original draft, Writing – review & editing, Visualization. **Kai K. Lie:** Conceptualization, Methodology, Software, Formal analysis, Writing – review & editing, Supervision, Project administration, Funding acquisition. **Anne-Katrine Lundebye:** Conceptualization, Formal analysis, Writing – review & editing, Supervision. **Liv Søfteland:** Conceptualization, Methodology, Formal analysis, Resources, Writing – review & editing, Supervision, Funding acquisition.

Declaration of competing interest

The authors declare that they have no known competing financial interests or personal relationships that could have appeared to influence the work reported in this paper.

Acknowledgement

The authors want to thank Maren Hoff Austgulen and Eva Mykkeltvedt at IMR for their assistance during the experimental work. This research was funded by the Research Council of Norway, grant 281032 HAVBRUK2: Tolerance of Atlantic salmon to novel feed mycotoxins - Implications on fish performance and nutrient interactions.

Appendix A. Supplementary data

Supplementary data to this article can be found online at https://doi.org/10.1016/j.fct.2022.112819.

References

Almeida, A.M., Bertoncini, C.R., Borecký, J., Souza-Pinto, N.C., Vercesi, A.E., 2006. Mitochondrial DNA damage associated with lipid peroxidation of the mitochondrial membrane induced by Fe2+-citrate. An Acad. Bras Ciências 78, 505–514.
Alonso-Garrido, M., Escrivá, L., Manyes, L., Font, G., 2018. Enniatin B induces expression changes in the electron transport chain pathway related genes in lymphoblastic T-cell line. Food Chem. Toxicol. 121, 437–443.
Andrews, N.C., 1999. The iron transporter DMT1. Int. J. Biochem. Cell Biol. 31, 991–994.
Bernal-Algaba, E., Pulgarín-Alfaro, M., Fernández-Cruz, M.L., 2021. Cytotoxicity of mycotoxins frequently present in aquafeeds to the fish cell line RTGill-W1. Toxins 13, 581.
Bernhoft, A., Eriksen, G., Sundheim, L., Berntssen, M., Brantsæter, A., Brodal, G., Fæste, C., Hofgaard, I., Rafoss, T., Sivertsen, T., 2013a. Risk Assessment of Mycotoxins in Cereal Grain in Norway. Opinion of the Scientific Steering Committee of the Norwegian Scientific Committee for Food Safety, Oslo, Norway.
Bernhoft, A., Eriksen, G.S., Sundheim, L., Berntssen, M., Brantsæter, A.L., Brodal, G., Fæste, C.K., Hofgaard, I.S., Rafoss, T., Sivertsen, T., 2013b. Risk Assessment of Mycotoxins in Cereal Grain in Norway. Opinion of the Scientific Steering Committee of the Norwegian Scientific Committee for Food Safety. VKM report.
Biasiotto, G., Di Lorenzo, D., Archetti, S., Zanella, I., 2016. Iron and neurodegeneration: is ferritinophagy the link? Mol. Neurobiol. 53, 5542–5574.
Brown, G.C., Murphy, M.P., Jastroch, M., Divakaruni, A.S., Mookerjee, S., Treberg, J.R., Brand, M.D., 2010. Mitochondrial proton and electron leaks. Essays Biochem. 47, 53–67.
Chandel, N.S., 2021. NADPH—the forgotten reducing equivalent. Cold Spring Harbor Perspect. Biol. 13, a040550.
Chinetti, G., Fruchart, J.-C., Staels, B., 2000. Peroxisome proliferator-activated receptors (PPARs): nuclear receptors at the crossroads between lipid metabolism and inflammation. Inflamm. Res. 49, 497–505.
Choi, A., Alam, J., 1996. Heme oxygenase-1: function, regulation, and implication of a novel stress-inducible protein in oxidant-induced lung injury. Am. J. Respir. Cell Mol. Biol. 15, 9–19.
Colombini, M., 2004. VDAC: the channel at the interface between mitochondria and the cytosol. Mol. Cell. Biochem. 256, 107–115.
Das, K., Roychoudhury, A., 2014. Reactive oxygen species (ROS) and response of antioxidants as ROS-scavengers during environmental stress in plants. Front. Environ. Sci. 2, 53.
Dixon, S.J., Lemberg, K.M., Lamprecht, M.R., Skouta, R., Zaitsev, E.M., Gleason, C.E., Patel, D.N., Bauer, A.J., Cantley, A.M., Yang, W.S., 2012. Ferroptosis: an iron-dependent form of nonapoptotic cell death. Cell 149, 1060–1072.
Dixon, S.J., Stockwell, B.R., 2014. The role of iron and reactive oxygen species in cell death. Nat. Chem. Biol. 10, 9–17.
Dodson, M., Castro-Portuguez, R., Zhang, D.D., 2019. NRF2 plays a critical role in mitigating lipid peroxidation and ferroptosis. Redox Biol. 23, 101107.
Dornetshuber, R., Heffeter, P., Sulyok, M., Schumacher, R., Chiba, P., Kopp, S., Koellensperger, G., Micksche, M., Lemmens-Gruber, R., Berger, W., 2009. Interactions between ABC-transport proteins and the secondary Fusarium metabolites enniatin and beauvericin. Mol. Nutr. Food Res. 53, 904–920.
Escrivá, L., Jennen, D., Caiment, F., Manyes, L., 2018. Transcriptomic study of the toxic mechanism triggered by beauvericin in Jurkat cells. Toxicol. Lett. 284, 213–221.
Ferrer, E., Juan-García, A., Font, G., Ruiz, M., 2009. Reactive oxygen species induced by beauvericin, patulin and zearalenone in CHO-K1 cells. Toxicol. Vitro 23, 1504–1509.
Fjelldal, P.G., Hansen, T.J., Wargelius, A., Ayllon, F., Glover, K.A., Schulz, R.W., Fraser, T.W., 2020. Development of supermale and all-male Atlantic salmon to research the vgll3 allele-puberty link. BMC Genet. 21, 1–13.
García-Herranz, V., Valdehita, A., Navas, J., Fernández-Cruz, M., 2019. Cytotoxicity against fish and mammalian cell lines and endocrine activity of the mycotoxins beauvericin, deoxynivalenol and ochratoxin-A. Food Chem. Toxicol. 127, 288–297.
Hajnóczky, G., Robb-Gaspers, L.D., Seitz, M.B., Thomas, A.P., 1995. Decoding of cytosolic calcium oscillations in the mitochondria. Cell 82, 415–424.
Hannou, S.A., Haslam, D.E., Mckeown, N.M., Herman, M.A., 2018. Fructose metabolism and metabolic disease. J. Clin. Invest. 128, 545–555.
Hilgenfeld, R., Saenger, W., 1985. Structural Chemistry of Natural and Synthetic Ionophores and Their Complexes with Cations. Host Guest Complex Chemistry/Macrocycles. Springer.
Hooft, J.M., Encarnação, P., Bureau, D.P., 2011. Rainbow trout (Oncorhynchus mykiss) is extremely sensitive to the feed-borne Fusarium mycotoxin deoxynivalenol (DON). Aquaculture 311, 224–232.
Hou, W., Xie, Y., Song, X., Sun, X., Lotze, M.T., Zeh III, H.J., Kang, R., Tang, D., 2016. Autophagy promotes ferroptosis by degradation of ferritin. Autophagy 12, 1425–1428.
Hussein, H.S., Brasel, J.M., 2001. Toxicity, metabolism, and impact of mycotoxins on humans and animals. Toxicology 167, 101–134.
Iso, I., 2009. 10993–5: 2009 Biological Evaluation of Medical Devices—Part 5: Tests for in Vitro Cytotoxicity. International Organization for Standardization, Geneva.
Ivanov, V., Evstratov, A., Sumskaya, L., Melnik, E., Chumburidze, T., Portnova, S., Balashova, T., Ovchinnikov, Y.A., 1973. Sandwich complexes as a functional form of the enniatin ionophores. FEBS Lett. 36, 65–71.
Ivanova, L., Egge-Jacobsen, W., Solhaug, A., Thoen, E., Fæste, C., 2012. Lysosomes as a possible target of enniatin B-induced toxicity in Caco-2 cells. Chem. Res. Toxicol. 25, 1662–1674.
Jestoi, M., 2008. Emerging Fusarium-mycotoxins fusaproliferin, beauvericin, enniatins, and moniliformin—a review. Crit. Rev. Food Sci. Nutr. 48, 21–49.
Jiang, X., Stockwell, B.R., Conrad, M., 2021. Ferroptosis: mechanisms, biology and role in disease. Nat. Rev. Mol. Cell Biol. 1–17.
Jonsson, M., Jestoi, M., Anthoni, M., Welling, A., Loivamaa, I., Hallikainen, V., Kankainen, M., Lysøe, E., Koivisto, P., Peltonen, K., 2016. Fusarium mycotoxin enniatin B: cytotoxic effects and changes in gene expression profile. Toxicol. Vitro 34, 309–320.
Ju, J., Song, Y.-N., Wang, K., 2021. Mechanism of ferroptosis: a potential target for cardiovascular diseases treatment. Aging Dis. 12, 261.
Kamyar, M., Rawnduzi, P., Studenik, C.R., Kouri, K., Lemmens-Gruber, R., 2004. Investigation of the electrophysiological properties of enniatins. Arch. Biochem. Biophys. 429, 215–223.
Kholodenko, B.N., 2006. Cell-signalling dynamics in time and space. Nat. Rev. Mol. Cell Biol. 7, 165–176.
Kim, D., Langmead, B., Salzberg, S.L., 2015. HISAT: a fast spliced aligner with low memory requirements. Nat. Methods 12, 357–360.
Klarić, M.Š., Pepeljnjak, S., Domijan, A.M., Petrik, J., 2007. Lipid peroxidation and glutathione levels in porcine kidney PK15 cells after individual and combined treatment with fumonisin B1, beauvericin and ochratoxin A. Basic Clin. Pharmacol. Toxicol. 100, 157–164.
Klover, P.J., Mooney, R.A., 2004. Hepatocytes: critical for glucose homeostasis. Int. J. Biochem. Cell Biol. 36, 753–758.
Kouri, K., Duchen, M.R., Lemmens-Gruber, R., 2005. Effects of beauvericin on the metabolic state and ionic homeostasis of ventricular myocytes of the Guinea pig. Chem. Res. Toxicol. 18, 1661–1668.
Kouri, K., Lemmens, M., Lemmens-Gruber, R., 2003. Beauvericin-induced channels in ventricular myocytes and liposomes. Biochim. Biophys. Acta Biomembr. 1609, 203–210.
Leaver, M.J., Bautista, J.M., Björnsson, B.T., Jönsson, E., Krey, G., Tocher, D.R., Torstensen, B.E., 2008. Towards fish lipid nutrigenomics: current state and prospects for fin-fish aquaculture. Rev. Fish. Sci. 16, 73–94.
Liao, Y., Smyth, G.K., Shi, W., 2014. featureCounts: an efficient general purpose program for assigning sequence reads to genomic features. Bioinformatics 30, 923–930.
Lieber, C.S., 2002. S-adenosyl-L-methionine: its role in the treatment of liver disorders. Am. J. Clin. Nutr. 76, 1183S–1187S.
Lin, J., Huang, F., Liang, T., Qin, Q., Xu, Q., Huang, X., Zhang, J., Xiao, K., Zhu, H., Zhao, J., 2021. EPA and DHA confer protection against DON-induced endoplasmic reticulum stress and iron imbalance in IPEC-1 cells. Br. J. Nutr. 1–29.
Lindblad, M., Gidlund, A., Sulyok, M., Börjesson, T., Krska, R., Olsen, M., Fredlund, E., 2013. Deoxynivalenol and other selected Fusarium toxins in Swedish wheat—occurrence and correlation to specific Fusarium species. Int. J. Food Microbiol. 167, 284–291.
Love, M.I., Huber, W., Anders, S., 2014. Moderated estimation of fold change and dispersion for RNA-seq data with DESeq2. Genome Biol. 15, 1–21.
Lushchak, V.I., 2012. Glutathione homeostasis and functions: potential targets for medical interventions. J. Amino Acids 2012, 736837.

Magtanong, L., Ko, P.-J., To, M., Cao, J.Y., Forcina, G.C., Tarangelo, A., Ward, C.C., Cho, K., Patti, G.J., Nomura, D.K., 2019. Exogenous monounsaturated fatty acids promote a ferroptosis-resistant cell state. Cell Chem. Biol. 26, 420–432 e9.
Mallebrera, B., Brandolini, V., Font, G., Ruiz, M., 2015. Cytoprotective effect of resveratrol diastereomers in CHO-K1 cells exposed to beauvericin. Food Chem. Toxicol. 80, 319–327.
Mallebrera, B., Font, G., Ruiz, M., 2014. Disturbance of antioxidant capacity produced by beauvericin in CHO-K1 cells. Toxicol. Lett. 226, 337–342.
Mallebrera, B., Prosperini, A., Font, G., Ruiz, M.J., 2018. In vitro mechanisms of Beauvericin toxicity: a review. Food Chem. Toxicol. 111, 537–545.
Manoli, I., Alesci, S., Blackman, M.R., Su, Y.A., Rennert, O.M., Chrousos, G.P., 2007. Mitochondria as key components of the stress response. Trends Endocrinol. Metabol. 18, 190–198.
Melkonian, E.A., Asuka, E., Schury, M.P., 2021. Physiology, Gluconeogenesis [Online]. StatPearls Publishing. Available: https://www.ncbi.nlm.nih.gov/books/NBK541119/. (Accessed 19 October 2021).
Mena, N.P., Urrutia, P.J., Lourido, F., Carrasco, C.M., Núñez, M.T., 2015. Mitochondrial iron homeostasis and its dysfunctions in neurodegenerative disorders. Mitochondrion 21, 92–105.
Mendanha, S.A., Alonso, A., 2015. Effects of terpenes on fluidity and lipid extraction in phospholipid membranes. Biophys. Chem. 198, 45–54.
Moldal, T., Bernhoft, A., Rosenlund, G., Kaldhusdal, M., Koppang, E.O., 2018. Dietary deoxynivalenol (DON) may impair the epithelial barrier and modulate the cytokine signaling in the intestine of Atlantic salmon (Salmo salar). Toxins 10, 376.
Muñoz, Y., Carrasco, C.M., Campos, J.D., Aguirre, P., Núñez, M.T., 2016. Parkinson's Disease: the Mitochondria-Iron Link. Parkinson's disease, 2016.
Mwihia, E.W., Lyche, J.L., Mbuthia, P.G., Ivanova, L., Uhlig, S., Gathumbi, J.K., Maina, J. G., Eshitera, E.E., Eriksen, G.S., 2020. Co-occurrence and levels of mycotoxins in fish feeds in Kenya. Toxins 12, 627.
Nicholson, C.K., Lambert, J.P., Molkentin, J.D., Sadoshima, J., Calvert, J.W., 2013. Thioredoxin 1 is essential for sodium sulfide–mediated cardioprotection in the setting of heart failure. Arterioscler. Thromb. Vasc. Biol. 33, 744–751.
Oliveros, J.C., 2007. VENNY. An interactive tool for comparing lists with Venn Diagrams. *http://bioinfogp.cnb.csic.es/tools/venny/index.html*.
Ørnsrud, R., Silva, M.S., Berntssen, M.H., Lundebye, A.-K., Storesund, J.E., Lie, K.K., Waagbø, R., Sele, V., 2020. Program for overvåking av fiskefôr-Årsrapport for prøver innsamlet i 2019. *Rapport fra havforskningen*.
Ou, Y., Wang, S.-J., Li, D., Chu, B., Gu, W., 2016. Activation of SAT1 engages polyamine metabolism with p53-mediated ferroptotic responses. Proc. Natl. Acad. Sci. Unit. States Am. 113, E6806–E6812.
Paul, B.T., Manz, D.H., Torti, F.M., Torti, S.V., 2017. Mitochondria and Iron: current questions. Expet Rev. Hematol. 10, 65–79.
Prosperini, A., Berrada, H., Ruiz, M.J., Caloni, F., Coccini, T., Spicer, L.J., Perego, M.C., Lafranconi, A., 2017. A review of the mycotoxin enniatin B. Front. Public Health 5, 304.
Prosperini, A., Juan-García, A., Font, G., Ruiz, M., 2013a. Beauvericin-induced cytotoxicity via ROS production and mitochondrial damage in Caco-2 cells. Toxicol. Lett. 222, 204–211.
Prosperini, A., Juan-García, A., Font, G., Ruiz, M., 2013b. Reactive oxygen species involvement in apoptosis and mitochondrial damage in Caco-2 cells induced by enniatins A, A1, B and B1. Toxicol. Lett. 222, 36–44.
Qi, X., Yang, X., Chen, S., He, X., Dweep, H., Guo, M., Cheng, W.-H., Xu, W., Luo, Y., Gretz, N., 2014. Ochratoxin A induced early hepatotoxicity: new mechanistic insights from microRNA, mRNA and proteomic profiling studies. Sci. Rep. 4, 1–14.
Rowsell, E.V., Al-Tai, A.H., Carnie, J.A., Rowsell, K.V., 1973. Increased liver l-serine–pyruvate aminotransferase activity under gluconeogenic conditions. Biochem. J. 134, 349–351.
Salido, E., Pey, A.L., Rodriguez, R., Lorenzo, V., 2012. Primary hyperoxalurias: disorders of glyoxylate detoxification. Biochim. Biophys. Acta (BBA) - Mol. Basis Dis. 1822, 1453–1464.
Sanden, M., Hemre, G., Måge, A., Lunestad, B., Espe, M., Lie, K., Lundebye, A., Amlund, H., Waagbø, R., Ørnsrud, R., 2017. Program for Overvåking Av Fiskefôr Årsrapport for Prøver Innsamlet I 2016. NIFES, Bergen.
Sele, V., Sanden, M., Berntssen, M., Lunestad, B., Espe, M., Lie, K., Amlund, H., Lundebye, A., Hemre, G., Waagbø, R., Ørnsrud, R., 2018. Program for overvåking av fiskefôr - Årsrapport for prøver innsamlet i 2017. *Rapport fra havforskningen*.
Sele, V., Sanden, M., Berntssen, M., Storesund, J.E., Lie, K.K., Espe, M., Lundebye, A.-K., Hemre, G.I., Waagbø, R., Ørnsrud, R., 2019. Program for overvåking av fiskefôr-Årsrapport for prøver innsamlet i 2018. *Rapport fra havforskningen*.
Søfteland, L., Eide, I., Olsvik, P.A., 2009. Factorial design applied for multiple endpoint toxicity evaluation in Atlantic salmon (Salmo salar L.) hepatocytes. Toxicol. Vitro 23, 1455–1464.
Stanton, R.C., 2012. Glucose-6-phosphate dehydrogenase, NADPH, and cell survival. IUBMB Life 64, 362–369.
Stockwell, B.R., Jiang, X., Gu, W., 2020. Emerging mechanisms and disease relevance of ferroptosis. Trends Cell Biol. 30, 478–490.
Sun, Y., Li, W., Shen, S., Yang, X., Lu, B., Zhang, X., Lu, P., Shen, Y., Ji, J., 2019. Loss of alanine-glyoxylate and serine-pyruvate aminotransferase expression accelerated the progression of hepatocellular carcinoma and predicted poor prognosis. J. Transl. Med. 17, 1–16.
Tang, B.L., 2019. Neuroprotection by glucose-6-phosphate dehydrogenase and the pentose phosphate pathway. J. Cell. Biochem. 120, 14285–14295.
Terman, A., Kurz, T., 2013. Lysosomal iron, iron chelation, and cell death. Antioxidants Redox Signal. 18, 888–898.
Tolosa, J., Font, G., Mañes, J., Ferrer, E., 2017. Mitigation of enniatins in edible fish tissues by thermal processes and identification of degradation products. Food Chem. Toxicol. 101, 67–74.
Tolosa, J., Font, G., Mañes, J., Ferrer, E., 2014. Natural occurrence of emerging Fusarium mycotoxins in feed and fish from aquaculture. J. Agric. Food Chem. 62, 12462–12470.
Tomoda, H., Huang, X.H., Cao, J., Nishida, H., Nagao, R., Okuda, S., Tanaka, H., Omura, S., Arai, H., Inoue, K., 1992. Inhibition of acyl-CoA: cholesterol acyltransferase activity by cyclodepsipeptide antibiotics. J. Antibiot. (Tokyo) 45, 1626–1632.
Tonshin, A.A., Teplova, V.V., Andersson, M.A., Salkinoja-Salonen, M.S., 2010. The Fusarium mycotoxins enniatins and beauvericin cause mitochondrial dysfunction by affecting the mitochondrial volume regulation, oxidative phosphorylation and ion homeostasis. Toxicology 276, 49–57.
Vaclavikova, M., Malachova, A., Veprikova, Z., Dzuman, Z., Zachariasova, M., Hajslova, J., 2013. 'Emerging'mycotoxins in cereals processing chains: changes of enniatins during beer and bread making. Food Chem. 136, 750–757.
Van der meeren, L., Verduijn, J., Krysko, D.V., Skirtach, A.G., 2020. AFM analysis enables differentiation between apoptosis, necroptosis, and ferroptosis in murine cancer cells. iScience 23, 101816.
Williams, D.E., 2012. The rainbow trout liver cancer model: response to environmental chemicals and studies on promotion and chemoprevention. Comp. Biochem. Physiol. C Toxicol. Pharmacol. 155, 121–127.
Wu, G., Fang, Y.-Z., Yang, S., Lupton, J.R., Turner, N.D., 2004. Glutathione metabolism and its implications for health. J. Nutr. 134, 489–492.
Wu, Q., Patocka, J., Nepovimova, E., Kuca, K., 2018. A review on the synthesis and bioactivity aspects of beauvericin, a Fusarium mycotoxin. Front. Pharmacol. 9, 1338.
Xie, Y., Hou, W., Song, X., Yu, Y., Huang, J., Sun, X., Kang, R., Tang, D., 2016. Ferroptosis: process and function. Cell Death Differ. 23, 369–379.
Ytrestøyl, T., Aas, T.S., Åsgård, T., 2015. Utilisation of feed resources in production of Atlantic salmon (Salmo salar) in Norway. Aquaculture 448, 365–374.
Yuan, H., Li, X., Zhang, X., Kang, R., Tang, D., 2016. Identification of ACSL4 as a biomarker and contributor of ferroptosis. Biochem. Biophys. Res. Commun. 478, 1338–1343.
Zhan, X., Long, Y., Zhan, X., Mu, Y., 2017. Consideration of statistical vs. biological significances for omics data-based pathway network analysis. Med One 2.
Zhang, F., Tao, Y., Zhang, Z., Guo, X., An, P., Shen, Y., Wu, Q., Yu, Y., Wang, F., 2012. Metalloreductase Steap3 coordinates the regulation of iron homeostasis and inflammatory responses. Haematologica 97, 1826.
Zhao, L., Feng, Y., Xu, Z.-J., Zhang, N.-Y., Zhang, W.-P., Khalil, M.M., Sun, L.-H., 2021. Selenium mitigated aflatoxin B1-induced cardiotoxicity with potential regulation of 4 selenoproteins and ferroptosis signaling in chicks. Food Chem. Toxicol. 112320.
Zhao, M., Shi, J., Zhao, Z., Zhou, D., Dong, S., 2018. Enhancing chlorophenol biodegradation: using a co-substrate strategy to resist photo-H2O2 stress in a photocatalytic-biological reactor. Chem. Eng. J. 352, 255–261.